Hindawi Publishing Corporation
Journal of Nanomaterials
Volume 2014, Article ID 291964, 8 pages
http://dx.doi.org/10.1155/2014/291964

Research Article

One-Pot Synthesis of Cu_2O/Cu Self-Assembled Hollow Nanospheres with Enhanced Photocatalytic Performance

Bo Zhou,[1] Zhiguo Liu,[2] Haijun Zhang,[1] and Yan Wu[1]

[1] *Engineering Research Academy of Graphite New Materials, Heilongjiang University of Science and Technology, Harbin 150027, China*
[2] *Department of Physics, Harbin Institute of Technology, Harbin 150080, China*

Correspondence should be addressed to Bo Zhou; apenbox@126.com and Zhiguo Liu; liuzhiguo@hit.edu.cn

Received 16 December 2013; Revised 27 January 2014; Accepted 28 January 2014; Published 27 February 2014

Academic Editor: Chuanfei Guo

Cu_2O/Cu hollow spheres are prepared using one-pot template-free solvent-thermal synthesis route with $(CH_3COO)_2Cu{\cdot}H_2O$ as a precursor. With the reaction time increasing gradually from 2 h to 20 h, the morphology of the Cu_2O/Cu evolves from nanoparticle to hollow nanosphere. The hollow structure is obtained when the cooling rate falls down to 0.7°C/min. And the content of Cu in the hollow spheres also can be easily controlled by adjusting the solvent-thermal synthesis time. Using photocatalytic degradation of phenol as the probe molecules under visible-light illumination, we have investigated the influence of hollow structure on the photocatalytic activity of Cu_2O/Cu. The prepared hollow sphere Cu_2O/Cu particles exhibited a higher photodegradation capability than nanoparticles and solid spheres. When the content of Cu lies in the range of 11–86 wt%, the samples exhibit higher photocatalytic performance, indicating that the Cu_2O/Cu particles with hollow structure are promising candidates for the processing of pollutants.

1. Introduction

Semiconductor-based photocatalysts, activated by illumination at room temperature, are used for degradation of organic pollutants by redox reaction. The technique is environmentally clean and thus attracts more and more attention [1]. As is well known, the activity of a catalyst depends largely on geometry and morphology. Hollow/porous structures possess large area of surface and interface, which enhances not only the adsorption and desorption of products but also light harvesting, thereby improves the catalytic activity. Some existing works have demonstrated that morphology of materials can be well controlled in some important photocatalytic materials [2–5]. Various method have been developed to achieve these special structures, which involve hard templates or soft templates (PEG [6], CTAB [7]), as well as physical/chemical processes based on Kirkendall effect [8], Ostwald ripening [9], oriented attachment [10], and so forth. Although much progress has been made in the synthesis of hollow spheres, it remains a major challenge to develop a fast and facile solution route for the preparation of inorganic hollow nanostructures, especially one-pot synthesis nanocomposite with hollow structure.

As is well known, the maximum irradiation of sunlight lies in the visible range, and only photocatalysts with corresponding band gap could sufficiently use solar energy. The band gap of Cu_2O is 2.0~2.2 eV, and the component elements are inexpensive and abundantly available, making it a promising candidate for photocatalysts. Numerous reports have shown the superior performance of Cu_2O on solar energy conversion [11], photocatalytic degradation of organic pollutants [12], and decomposition of water into H_2 and O_2 [13]. In recent years, various Cu_2O hollow structures have been prepared by different methods. Qi and coworkers reported the one-pot synthesis of octahedral Cu_2O nanocages via a catalytic solution route. Zeng et al. reported the preparation of hollow nanocubes of Cu_2O via reductive self-assembly of CuO nanocrystals. In both synthetic processes, expensive and toxic organic solvents were used. Although many efforts have been devoted to synthesizing hollow Cu_2O, few results were reported on the synthesis and photocatalytic property of Cu_2O/Cu with hollow structure. We have previously reported

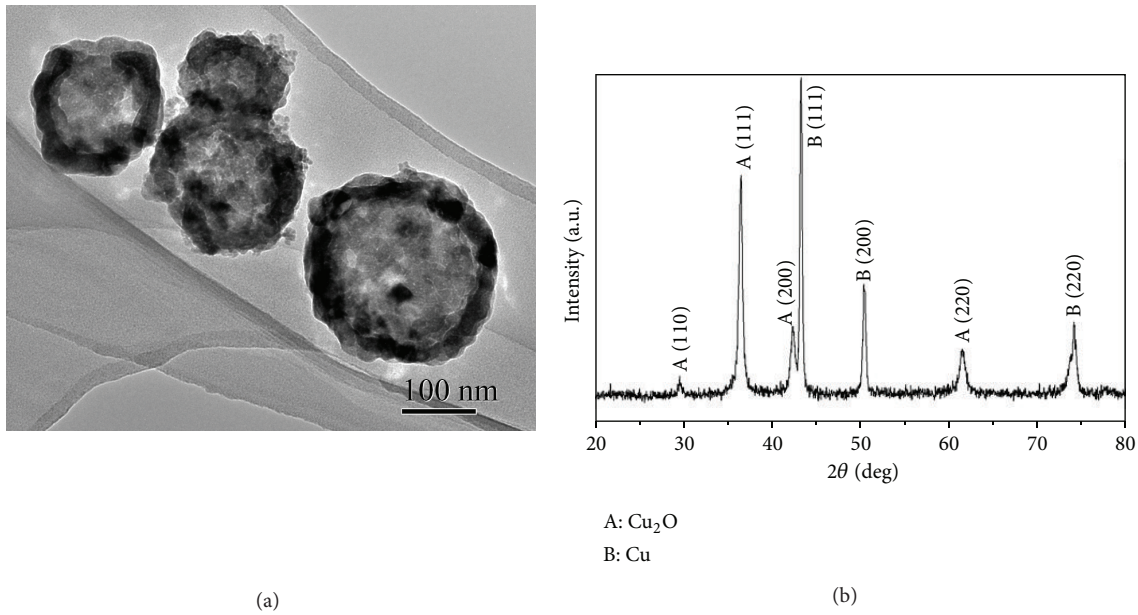

Figure 1: (a) TEM images of sample S4; (b) XRD patterns of sample S4.

that the composite of Cu_2O/Cu has higher photocatalytic activity than simple-phase Cu_2O [14]. It remains a great challenge to develop a feasible method for the synthesis of nanocomposite of Cu_2O/Cu structures with hollow morphologies.

A simple and green one-pot in situ synthetic route for nanosized Cu_2O/Cu hollow nanospheres is introduced here. The synthesis of Cu_2O/Cu is developed with a template-free solvent-thermal route to control its morphology and phase composition. More importantly, the hollow structure of Cu_2O/Cu can be obtained by adjusting the reaction conditions. A possible formation mechanism was proposed to account for the production of hollow structures. The effect of reaction time and cooling rate on its morphology was investigated. The adsorption and photocatalytic activity of samples were evaluated by the photocatalytic degradation of phenol under visible light illumination.

2. Experimental

2.1. Preparation of Cu_2O/Cu Hollow Spheres. All the chemicals were analytical grade regents used without further purification. In a typical preparation, copper acetate ($(CH_3COO)_2Cu{\cdot}H_2O$, 0.02–0.05 M) was dissolved in a mixed organic solvent of N,N-dimethylformamide (DMF) and ethanol. After the solution was stirred for 30 min, 35 mL of this transparent blue solvent was sealed in a Teflon-lined stainless steel autoclave with a capacity of 50 mL and heated at 200°C for 2–20 h in electric oven. After reaction, the precipitation was separated from the solution by centrifugation, then washed with alcohol for several times, and finally dried at 70°C for 5 h in a vacuum oven. The denotations of samples prepared at different condition are shown in Table 1.

2.2. Characterization. The samples were characterized by X-ray powder diffraction (XRD) using a Rigaku 12 kW X-ray diffractometer with Cu K_α radiation (λ = 0.15418 nm). Their morphology and size distribution were inspected with a JEM-S4800 field-emission scanning electron microscope (FESEM) operated at 15 Kv and a JEOL-2010 transmission electron microscope (TEM) working at 200 kV. N_2 adsorption-desorption isotherms were obtained using a Quantachrome Autosorb-1 apparatus. Barret-Joyner-Halenda (BJH) method was employed to determine the pore diameter (d_P) and pore volume (V_P). The specific surface area (S_{BET}) was calculated using the Brunauer-Emmett-Teller (BET) method.

2.3. Measurement of Adsorption and Photocatalytic Activity. The adsorption behavior and photocatalytic activity of the Cu_2O/Cu were evaluated by the degradation of the solution of phenol at a concentration of 10 mg/L. 0.030 g Cu_2O/Cu NCs powder was dispersed in a 50 mL probe molecular aqueous solution. Before illumination, the suspension was stirred in the dark for more than 120 min to achieve an adsorption/desorption equilibrium of organic molecules on the surface of Cu_2O/Cu. The photocatalytic reaction was carried out at room temperature by using a 100 W tungsten lamp as a visible light source. At different time intervals during the experiment, 5 mL of solution was sampled each time for analysis. After centrifugation at 11000 rpm for 10 min, the absorbance of solution was measured using a UV-visible spectrophotometer (TU-1901).

3. Results and Discussions

3.1. Structure and Morphology. Sample S4 (precursor concentration is 0.02 M, reaction time is 14 h, and cooling rate is 0.7°C/min) possesses the typical morphology of all, whose TEM images are shown in Figure 1(a). Hollow spherical nanoparticles are observed, with the diameter of 140~280 nm, whose shell is 30~50 nm in thickness. It can be seen from

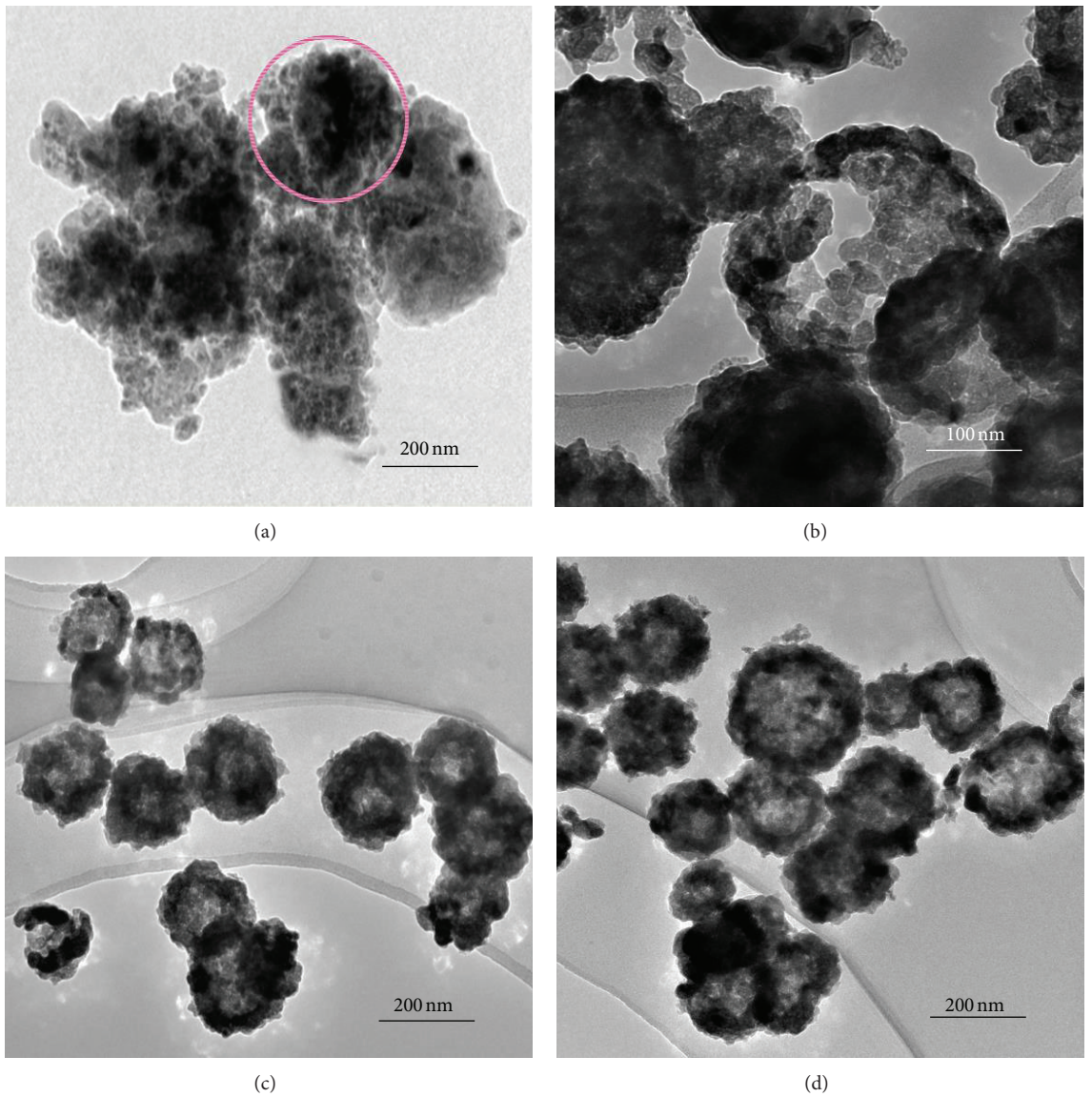

Figure 2: The effect of reaction time on the formation of Cu_2O/Cu hollow nanospheres: (a) 2 h; (b) 4 h; (c) 10 h; and (d) 20 h.

Table 1: Experimental conditions, phase composition, and characterized parameters of different samples, where S_{BET}, d_P, and V_P are specific surface area, pore diameter, and pore volume, respectively.

Sample	Reaction time (h)	Cu wt%	Cu_2O wt%	S_{BET} (m^2/g)	d_P (nm)	V_P (cm^3/g)
S1	2	—	100	12.5	2.162	0.0131
S2	6	11	89	17.4	1.688	0.0161
S3	10	31	67	18.9	1.774	0.0154
S4	14	61	39	19.3	2.088	0.0304
S5	20	86	14	19.1	2.134	0.0234

Figure 1(b) that this sample is composite materials, which are characterized by the two sets of diffraction peaks, that is, Cu_2O (space group Pn3 m; a0 = 0.4252 nm; JCPDS 05-0667) and cubic Cu (space group Fm3m; a0 = 0.3613 nm; JCPDS 04-0836). The peaks located at 29.58°, 36.43°, 42.37°, 64.45°, and 73.66° can be, respectively, identified as Cu_2O (110), (111), (200), (220), and (311) diffraction plane. And the peaks located at 43.34°, 50.53°, and 74.21° can be, respectively, identified as Cu (111), (200), and (220) diffraction plane.

To study the formation process of the Cu_2O hollow spheres, samples were collected at different reaction time and were characterized by the TEM analysis (Figure 2). When the solution at 200°C for 2 h, the system appears brown precipitate; these are nanoparticles that can be seen

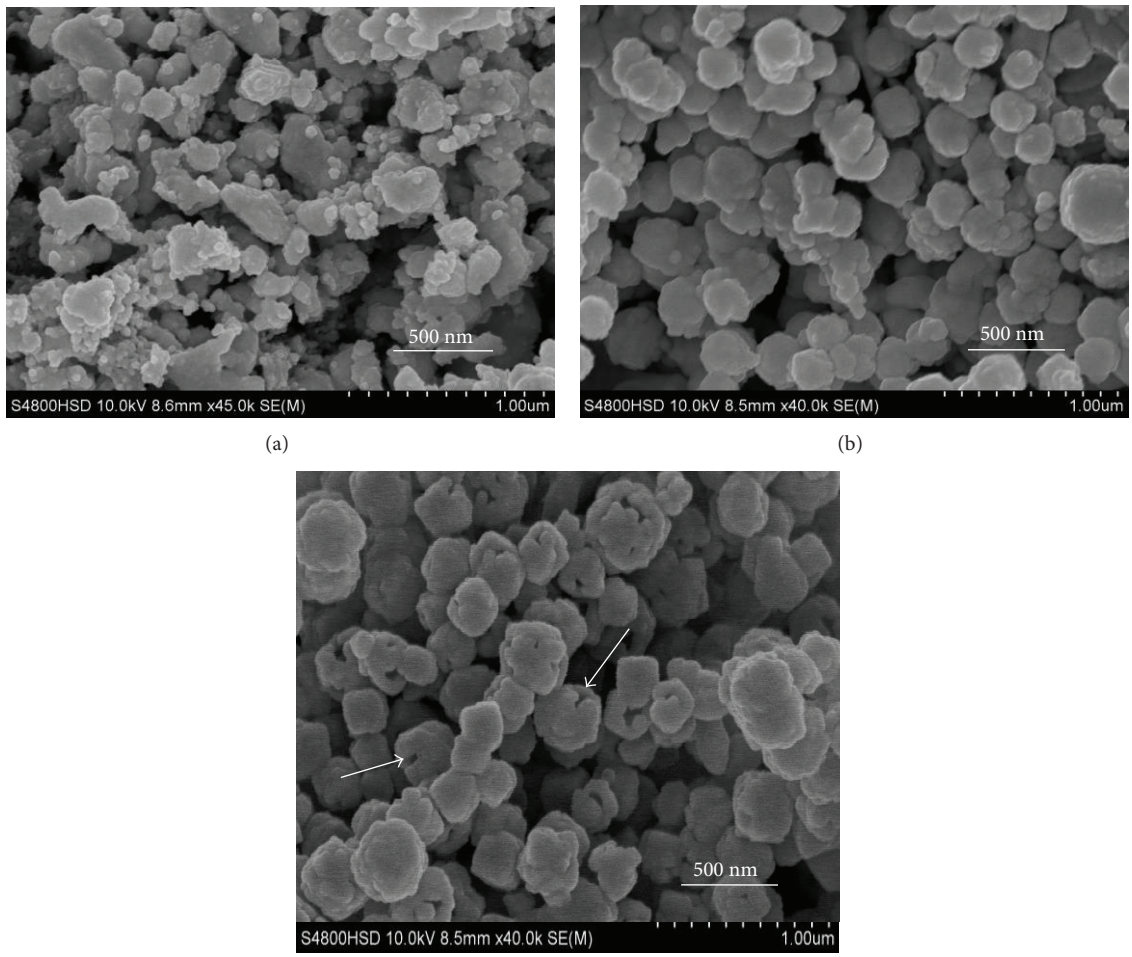

Figure 3: The cooling rate-dependent morphology: (a) quenched in ice water; (b) 3°C/min; and (c) 0.7°C/min.

from Figure 2(a). Figure 2(b) is a TEM image of the sample collected after 4 h, showing that Cu_2O nanoparticles aggregated to form loose spheres, whose diameter are approximately 140–280 nm and part of them are hollow structure. When the reaction time increases to 10 h, the spherical self-assembled internal nanoparticles are significantly decreased; hollow structure can be seen from Figure 2(c), a thin-wall hollow spherical structure was formed, which diameter is approximately 180 nm and the wall thickness is about 30 nm. When the reaction time is 20 h, the color of the sample is completely changed to dark purple. The corresponding TEM photograph is shown in Figure 2(d), and the hollow structure obtained exhibits no change in morphology. This time-dependent self-assembly allows selective synthesis of hollow mesoporous spheres by changing reaction time, which is of great importance for designing catalysts with high activity.

In this experiment, the authors found that the cooling rate has great impact on the formation of hollow structure. Figure 3 shows the SEM of samples obtained at 200°C for 10 h with different cooling rate. Shown in the Figure 3(a) is the sample obtained when the stainless steel autoclave was quenched in ice water, the morphology of which is disorganized nanoparticles. Decreasing the cooling rate to 3°C/min (Figure 3(b)), the product exhibits spherical aggregated structure. When the cooling rate was decreased to 0.7°C/min, the hollow spheric structure with 140–280 nm diameter was formed, which could be indicated by the light and shade contrast as the arrow point inset Figure 3(c).

Figure 4 illustrates the Schematic formation process of Cu_2O/Cu hollow nanospheres. As indicated, the solid spheres are comprised of numerous smaller crystallites. Firstly, the nanocrystals formed and then driven by the minimization of the system energy; the small nanocrystals tend to aggregate together to form solid spherical groups. These aggregates exhibit various packing densities along the radial direction. With increasing reaction time, Ostwald ripening [9] then comes into effect; the particles with high surface energy move from the center to the surface. Voids in the cores of large aggregates gradually form and become bigger. The original driving force for this ripening is attributed to the existence of intrinsic density variations inside the starting solid aggregates.

Figure 5 shows the XRD patterns of a series of samples prepared with different reaction time at 200°C. For the S1, all diffraction peaks can be indexed to be cubic phase of

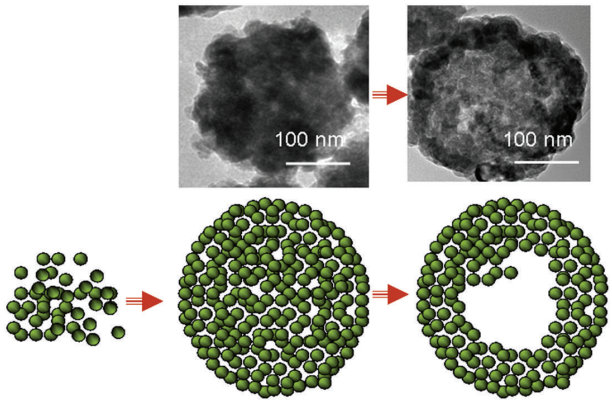

FIGURE 4: Schematic illustration of the formation hollow spheric nanostructures.

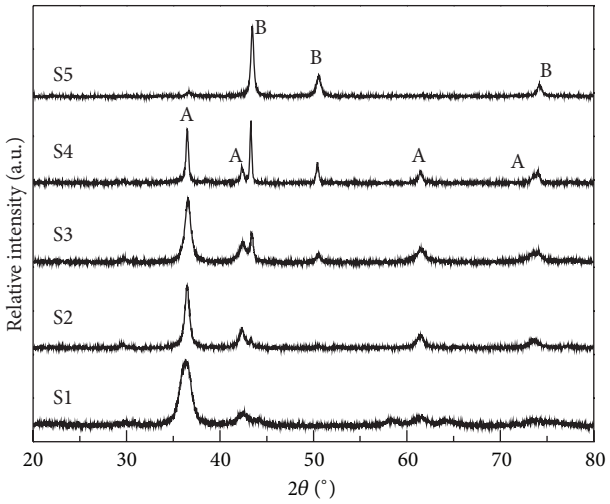

A: Cu_2O
B: Cu

FIGURE 5: Powder XRD patterns of hollow nanospheres synthesized with different reaction times: (S1) 4 h; (S2) 6 h; (S3) 10 h; (S4) 14 h; and (S5) 20 h.

Cu_2O crystal (JCPDS number 05-0667). When the reaction time was prolonged from 6 h to 20 h, the samples (S2, S3, S4, and S5) were found to be composite materials of Cu_2O and Cu. With increasing the reaction time, the relative intensity of Cu_2O (1 1 1) peak increases, indicating the higher content of Cu_2O in the NCs. (Table 1). With increasing precursor concentration, the relative intensity of Cu_2O (1 1 1) peak increases, indicating the higher content of Cu_2O in the nanocomposites. The mass fraction of Cu_2O in the nanocomposites can be calculated using the relative ratio [15]:

$$\frac{I_{Cu}}{I_{Cu_2O(111)} + I_{Cu(111)}}, \quad (1)$$

where $I_{Cu_2O(111)}$ and $I_{Cu(111)}$ are the height of the characteristic diffraction peaks of Cu_2O (111) and Cu (111) planes, respectively. As calculated from XRD results (Figure 5), the corresponding content of Cu increases from 0 wt% to 86 wt% when the time increases from 4 h (S1) to 20 h (S5). Thus, the reaction time plays a crucial role in forming different ratios of Cu_2O to Cu in the composite.

Figure 6 shows the relationship between the morphology and the precursor concentration. Obviously, the concentration of precursor has a great effect on the morphology. At low precursor concentration of 0.02 M (S2, Figure 6(a)), hollow sphere is formed, whose diameter is approximately 140–280 nm. The contrast of light and shade can infer the possible hollow structure (the arrow inset Figure 6(b)). When the precursor concentration increases to 0.05 M, the diameter of microsphere increase to 2 μm, and the spheres become merged together. Therefore, when the precursor concentration changed, the products changed not only in size but also in morphology of the grain.

3.2. N_2 Adsorption-Desorption. Figure 7 show the N_2 adsorption-desorption isotherm of S1 and S4 (S4 is representative for all the hollow spheric samples), and the two adsorption isotherms all exhibit type IV hysteresis, indicating S1 and S4 are porous structures. The corresponding parameters are listed in Table 1. The pore size of S1 (inset Figure 7(a)) ranges from 33 to 42 nm, which can be attributed to the aggregation of nanoparticles. But for S4 (inset Figure 7(b)), the pore size has shown the obvious bimodal pore size distribution, which is located in the microporous and mesoporous region, respectively, including the maximum probability diameter of 3.7-3.8 nm between the interior of the particle agglomeration hole and 17–40 nm agglomeration piled holes between particles.

3.3. Photocatalytic Activity. Phenol is transparent to visible light and very hard to mineralize due to its resonance stability. The strong absorption peak at about 269 nm is selected to monitor the photocatalytic degradation process. With longer irradiation time, this characteristic peak becomes weaker and weaker, indicating the degradation of phenol. No new adsorption peaks appear and no obvious shift of the characteristic peak is observed, indicating the degradation of phenol.

In order to understand the hollow structure in enhancing the photocatalytic performance of Cu_2O, pure Cu_2O nanoparticles, nanospheres, and hollow nanospheres are prepared and the photocatalytic activity is studied. Shown in Figure 8 is the photocatalytic activity of Cu_2O with different morphologies, which is characterized by the initial concentration (C_0) and the concentrations at different time interval (C). The sizes of Cu_2O nanoparticle in the hollow spheres and nanospheres are approximately the same as the nanoparticles Cu_2O. From Figure 8, we can see that without catalyst, phenol cannot be degraded under visible light irradiation, whereas it can be easily degraded with the presence of Cu_2O photocatalysis. At an irradiation time of 120 min, 75% phenol is degraded with the presence of hollow spheric sample. On the contrary, the photocatalytic performance of nanoparticles and solid structure are relatively low; especially nanoparticles Cu_2O, the degradation rate is only 23%. Compared to solid

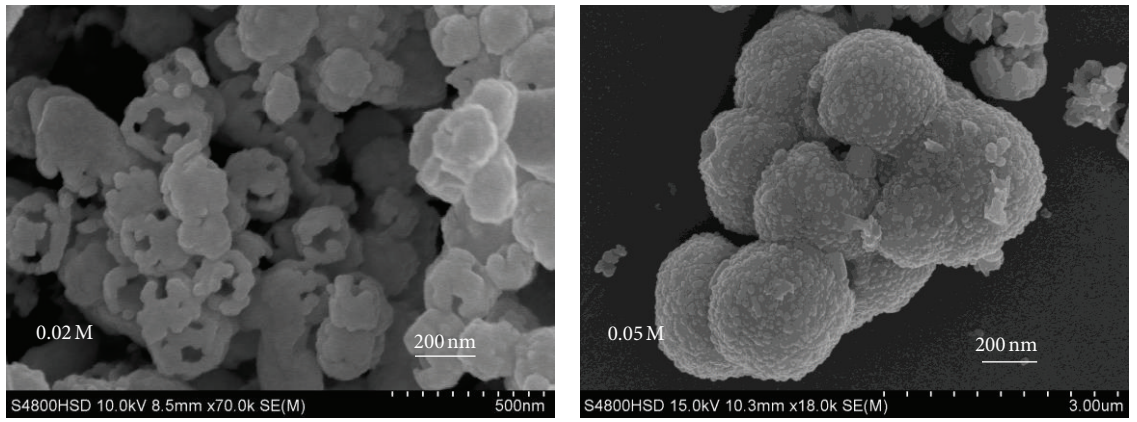

(a) (b)

Figure 6: SEM images of Cu_2O/Cu composites obtained in different precursor concentrations: (a) 0.02 M; (b) 0.05 M.

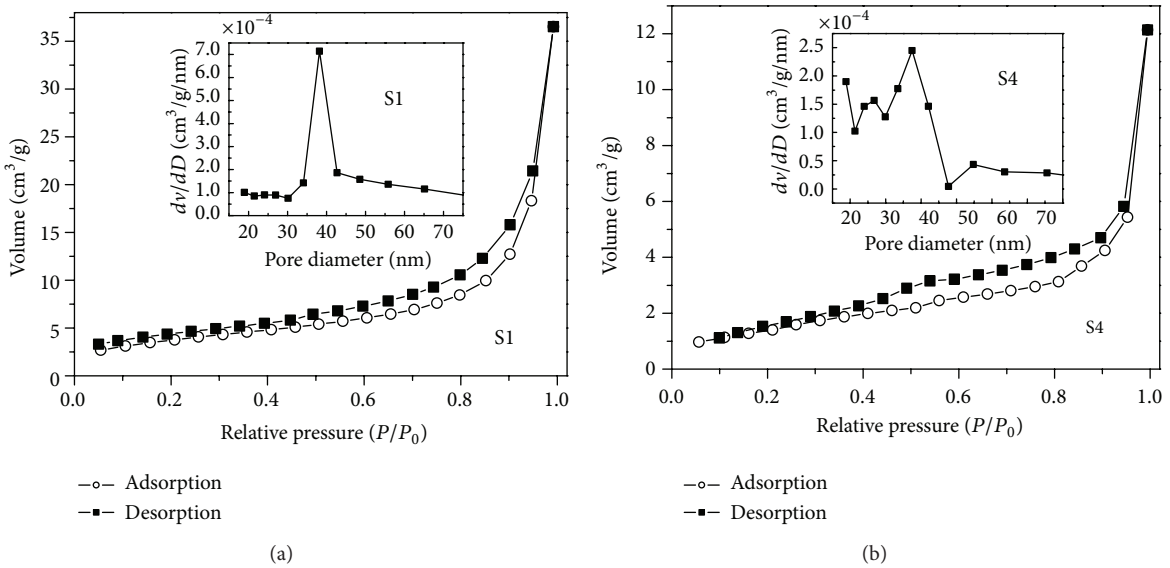

(a) (b)

Figure 7: N_2 adsorption-desorption BET isotherms of samples S1 and S4. The inset shows the pore size distribution.

particles, hollow structures have large specific surface areas, the interior and exterior surfaces, which enhance not only the adsorption and desorption of products but also light harvesting, thereby improving the catalytic activity.

Figure 9 shows the photocatalytic performance of Cu_2O/Cu hollow spheres, whose Cu contents are different. Among these samples, the performance of S1 is relatively low, while S3 exhibits the highest performance. As discussed above, S1 is the pure phase of Cu_2O and the other samples (S2–5) are nanocomposites of Cu_2O and Cu. The pure-phase semiconductor exhibits very low quantum efficiency due to the quick recombination of photoelectrons and holes [16]. According to the theory of metal/semiconductor heterostructure catalysis [17–21], the photocatalytic activity of semiconductor-based heterostructure depends greatly on the concentration of heterostructure interface and defect, which promotes interfacial charge-transfer kinetics between the metal and semiconductor and improves the separation of photogenerated electron-hole pairs, thus increasing photocatalytic activity [17]. In fact, a Schottky barrier was assumed to form at the Cu_2O and Cu interface; Cu acts as an electron sink that reduces the recombination of photoinduced electrons and holes (2). However, Cu_2O is known to absorb a relatively large amount of oxygen on the surface [22]. It has been proven that the electrons do accumulate on Cu particles, and the accumulation of electron on Cu will transfer to Cu_2O and O_2 will reduce O_2 to $^{\bullet}O_2^-$ (3), while the $^{\bullet}O_2^-$ oxidize the H_2O to form $^{\bullet}OH$ (4); finally, the organics have been degraded through the formation of $^{\bullet}OH$ (5) [23–25]. The accumulation of electron on photocatalyst will increase the rate of recombination. In Cu_2O/Cu, the interfaces between Cu and Cu_2O act as the sites where rapid seperation of photogenerated electrons and holes occurs. On the other hand, very high content of Cu (S5, 86 wt%) does not favor high photocatalytic activity, since Cu becomes a recombination center for electrons and holes instead [26]. Therefore, the mass fraction

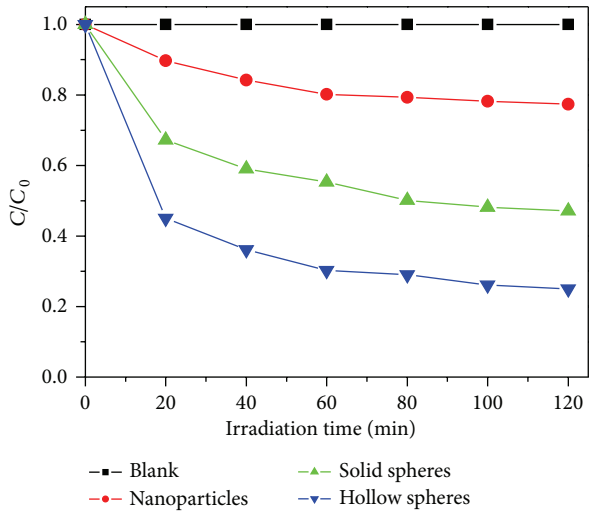

FIGURE 8: Relative concentration (C/C_0) of phenol versus time under visible light irradiation with Cu_2O nanoparticles, solid nanospheres, and hollow nanosphere as photocatalysts.

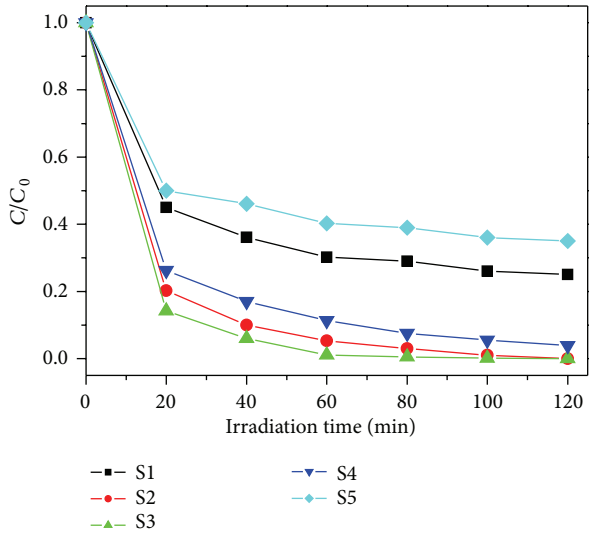

FIGURE 9: Relative concentration (C/C_0) of phenol versus time under visible light irradiation with the presence of hollow spheric Cu_2O/Cu NCs which have different Cu contents.

of Cu in the nanocomposites also influences photocatalytic activity.

Consider

$$\text{semiconductor} + h\nu \longrightarrow e^-_{CB} + h^+_{VB}, \quad (2)$$

$$e^-_{CB} + O_2 \longrightarrow {}^{\bullet}O_2^-, \quad (3)$$

$${}^{\bullet}O_2^- + H_2O \longrightarrow {}^{\bullet}OH, \quad (4)$$

$${}^{\bullet}OH + \text{organic} \longrightarrow \text{Degradation products}. \quad (5)$$

4. Conclusions

Hollow spheric Cu_2O/Cu photocatalysts have been synthesized by following a one-pot solvent-thermal synthesis route without using any templates and additives. The reaction time and cooling rate have a strong effect on the formation of the hollow Cu_2O/Cu nanospheres. The hollow spheric structure is formed at a reaction time in the range of 4 h to 20 h and low cooling rate 0.7°C/min. The content of Cu increases with increasing reaction time. As visible-light-driven photocatalysts, the hollow spheric Cu_2O/Cu exhibit better photocatalytic performance than the nanoparticles and solid spheres. Our route offers an effective way to control the synthesis of Cu_2O/Cu hollow spheres and may shed light on the design of simple route for one-pot synthesis of metal oxide nano-heterojunction, other well defined complex nanostructures.

Conflict of Interests

The authors declare that there is no conflict of interests regarding the publication of this paper.

Acknowledgments

This research work is funded by the National Science and Technology Support Program of China (no. 2013BAE04B03 and no. 2013BAE04B02) and the National Natural Science Foundation of China (no. 10674034).

References

[1] M. R. Hoffmann, S. T. Martin, W. Choi, and D. W. Bahnemann, "Environmental applications of semiconductor photocatalysis," *Chemical Reviews*, vol. 95, no. 1, pp. 69–96, 1995.

[2] L. M. Duan, Z. W. Quan, P. P. Yang, H. Wang, and J. Lin, "Shape-controlled synthesis of wurtzite ZnS microstructures under mild solvothermal condition," *Journal of Nanoscience and Nanotechnology*, vol. 9, no. 2, pp. 919–923, 2009.

[3] C. F. Guo, J. Zhang, M. Wang, Y. Tian, and Q. Liu, "Superstructures: a strategy to prepare wafer scale bismuth compound superstructures," *Small*, vol. 9, no. 14, pp. 2394–2398, 2013.

[4] C. F. Guo, J. Zhang, Y. Tian, and Q. Liu, "A general strategy to superstructured networks and nested self-similar networks of bismuth compounds," *ACS Nano*, vol. 6, pp. 8746–8752, 2012.

[5] C. F. Guo, S. Cao, J. Zhang et al., "Topotactic transformations of superstructures: from thin films to two-dimensional networks to nested two-dimensional networks," *Journal of the American Chemical Society*, vol. 133, no. 21, pp. 8211–8215, 2011.

[6] Y. Xu, D. Chen, X. Jiao, and K. Xue, "Nanosized Cu_2O/PEG400 composite hollow spheres with mesoporous shells," *Journal of Physical Chemistry C*, vol. 111, no. 44, pp. 16284–16289, 2007.

[7] H. Xu and W. Wang, "Template synthesis of multishelled Cu_2O hollow spheres with a single-crystalline shell wall," *Angewandte Chemie—International Edition*, vol. 46, no. 9, pp. 1489–1492, 2007.

[8] H. Goto, Y. Hanada, T. Ohno, and M. Matsumura, "Quantitative analysis of superoxide ion and hydrogen peroxide produced from molecular oxygen on photoirradiated TiO_2 particles," *Journal of Catalysis*, vol. 225, no. 1, pp. 223–229, 2004.

[9] H. G. Yang and H. C. Zeng, "Preparation of hollow anatase TiO_2 nanospheres via Ostwald ripening," *Journal of Physical Chemistry B*, vol. 108, no. 11, pp. 3492–3495, 2004.

[10] D. Li, M. H. Nielsen, J. R. I. Lee, C. Frandsen, J. F. Banfield, and J. J. de Yoreo, "Direction-specific interactions control crystal growth by oriented attachment," *Science*, vol. 336, pp. 1014–1018, 2012.

[11] A. Paracchino, J. C. Brauer, J.-E. Moser, E. Thimsen, and M. Graetzel, "Synthesis and characterization of high-photoactivity electrodeposited Cu_2O solar absorber by photoelectrochemistry and ultrafast spectroscopy," *Journal of Physical Chemistry C*, vol. 116, no. 13, pp. 7341–7350, 2012.

[12] G. Wua, W. Zhai, F. Sun, W. Chen, Z. Pan, and W. Li, "Morphology-controlled electrodeposition of Cu_2O microcrystalline particle films for application in photocatalysis under sunlight," *Materials Research Bulletin*, vol. 47, pp. 4026–4030, 2012.

[13] P. D. Tran, S. K. Batabyal, S. S. Pramana, J. Barber, L. H. Wong, and S. C. Loo, "A cuprous oxide-reduced graphene oxide (Cu_2O-rGO) composite photocatalyst for hydrogen generation: employing rGO as an electron acceptor to enhance the photocatalytic activity and stability of Cu_2O," *Nanoscale*, vol. 4, pp. 3875–3878, 2012.

[14] B. Zhou, H. Wang, Z. Liu et al., "Enhanced photocatalytic activity of flowerlike Cu_2O/Cu prepared using solvent-thermal route," *Materials Chemistry and Physics*, vol. 126, no. 3, pp. 847–852, 2011.

[15] Y. Chang, J. J. Teo, and H. C. Zeng, "Formation of colloidal CuO nanocrystallites and their spherical aggregation and reductive transformation to hollow Cu_2O nanospheres," *Langmuir*, vol. 21, no. 3, pp. 1074–1079, 2005.

[16] W. J. Foo, C. Zhang, and G. W. Ho, "Non-noble metal Cu-loaded TiO_2 for enhanced photocatalytic H_2 production," *Nanoscale*, vol. 5, pp. 759–764, 2013.

[17] H. Zhu, M. Du, D. Yu et al., "Selective growth of Au nanograins on specific positions (tips, edges and facets) of Cu_2O octahedrons to form Cu_2O-Au hierarchical heterostructures," *Dalton Transactions*, vol. 41, pp. 13795–13799, 2012.

[18] L. Kong, W. Chen, D. Ma, Y. Yang, S. Liu, and S. Huang, "Size control of Au@Cu_2O octahedra for excellent photocatalytic performance," *Journal of Materials Chemistry*, vol. 22, no. 2, pp. 719–724, 2012.

[19] K. Maeda and K. Domen, "Photocatalytic water splitting: recent progress and future challenges," *Journal of Physical Chemistry Letters*, vol. 1, no. 18, pp. 2655–2661, 2010.

[20] M. Yoshida, A. Yamakata, K. Takanabe, J. Kubota, M. Osawa, and K. Domen, "ATR-SEIRAS investigation of the fermi level of Pt cocatalyst on a GaN photocatalyst for hydrogen evolution under irradiation," *Journal of the American Chemical Society*, vol. 131, no. 37, pp. 13218–13219, 2009.

[21] D. Wang, X. Li, H. Li et al., "Semiconductor-noble metal hybrid nanomaterials with controlled structures," *Journal of Materials Chemistry A*, vol. 1, pp. 1587–1590, 2013.

[22] B. J. Wood, H. Wise, and R. S. Yolles, "Selectivity and stoichiometry of copper oxide in propylene oxidation," *Journal of Catalysis*, vol. 15, no. 4, pp. 355–362, 1969.

[23] W. Lu, S. Gao, and J. Wang, "One-pot synthesis of Ag/ZnO self-assembled 3D hollow microspheres with enhanced photocatalytic performance," *Journal of Physical Chemistry C*, vol. 112, no. 43, pp. 16792–16800, 2008.

[24] Y. Badr and M. A. Mahmoud, "Photocatalytic degradation of methyl orange by gold silver nano-core/silica nano-shell," *Journal of Physics and Chemistry of Solids*, vol. 68, no. 3, pp. 413–419, 2007.

[25] M. A. Mahmoud, W. Qian, and M. A. El-Sayed, "Following charge separation on the nanoscale in Cu_2O-Au nanoframe hollow nanoparticles," *Nano Letters*, vol. 11, no. 8, pp. 3285–3289, 2011.

[26] L. Ren, Y.-P. Zeng, and D. Jiang, "Preparation, characterization and photocatalytic activities of Ag-deposited porous TiO_2 sheets," *Catalysis Communications*, vol. 10, no. 5, pp. 645–649, 2009.